ORIGINAL PAPER

Utility of the two-source energy balance (TSEB) model in vine and interrow flux partitioning over the growing season

W. P. Kustas[1] · J. G. Alfieri[1] · H. Nieto[2] · T. G. Wilson[1] · F. Gao[1] · M. C. Anderson[1]

Abstract

For monitoring water use in vineyards, it becomes important to evaluate the evapotranspiration (ET) contributions from the two distinct management zones: the vines and the interrow. Often the interrow is not completely bare soil but contains a cover crop that is senescent during the main growing season (nominally May–August), which in Central California is also the dry season. Drip irrigation systems running during the growing season supply water to the vine plant and re-wet some of the surrounding bare soil. However, most of the interrow cover crop is dry stubble by the end of May. This paper analyzes the utility of the thermal-based two-source energy balance (TSEB) model for estimating daytime ET using tower-based land surface temperature (LST) estimates over two Pinot Noir (*Vitis vinifera*) vineyards at different levels of maturity in the Central Valley of California near Lodi, CA. The data were collected as part of the Grape Remote sensing Atmospheric Profile and Evapotranspiration eXperiment (GRAPEX). Local eddy covariance (EC) flux tower measurements are used to evaluate the performance of the TSEB model output of the fluxes and the capability of partitioning the vine and cover crop transpiration (T) from the total ET or T/ET ratio. The results for the 2014–2016 growing seasons indicate that TSEB output of the energy balance components and ET, particularly, over the daytime period yield relative differences with flux tower measurements of less than 15%. However, the TSEB model in comparison with the correlation-based flux partitioning method overestimates T/ET during the winter and spring through bud break, but then underestimates during the growing season. A major factor that appears to affect this temporal behavior in T/ET is the daily LAI used as input to TSEB derived from a remote sensing product. An additional source of uncertainty is the use of local tower-based LST measurements, which are not representative of the flux tower measurement source area footprint.

Introduction

The typical architecture of wine grape vineyards in California is characterized by widely spaced rows (~ 3 m) and tall plants (~ 2 m) with most of the biomass concentrated in the upper one-third to one-half of the plant. This wide row spacing and canopy architecture facilitates sunlight interception, air flow, and field operations. It also results in two distinct management zones: the vines and the interrow. Often, the treatment of these two management zones is

further complicated by a cover crop grown in the interrow. A remote sensing-based land surface model that captures the micro- and macro-scale exchanges between the vine, interrow and atmospheric boundary layer is needed to operationally monitor vineyard water use and both vine and interrow plant stress. The two-source energy balance (TSEB) formulation addresses the key factors affecting the convective and radiative exchange within the soil/substrate–plant canopy–atmosphere system.

As water supplies for agricultural production become more restricted due to overuse and drought, particularly in arid regions, there is a concerted effort to improve irrigation methods to reduce the amount of water lost through soil evaporation (E) versus transpiration (T). This is because for many crops T is correlated to biomass production and ultimately yield, while E provides little if any contribution from an agronomic point of view. While several measurement techniques have been developed to estimate T and E (Kool et al. 2014), they are very difficult to extrapolate from

✉ W. P. Kustas
Bill.Kustas@ars.usda.gov

1 USDA-ARS, Hydrology and Remote Sensing Laboratory, Beltsville, MD, USA

2 IRTA-Research and Technology Food and Agriculture, Lleida, Spain

the local patch scale to field scale, and certainly to landscape and regional scales. This study presents an application of the TSEB model for estimating evapotranspiration (ET) that explicitly partitions ET to T and E using land surface temperature (LST), which is also available from satellites, giving it a regional scale application.

In this paper, TSEB is applied using local tower LST observations representing conditions surrounding the eddy covariance flux tower. Both the total ET and the partitioned fluxes from vine and interrow systems estimated by TSEB are compared to eddy covariance ET. Additionally, for the 2014 and 2015 growing seasons, the T/ET ratio is estimated using the correlation-based flux partitioning method with the high-frequency eddy covariance data (Scanlon and Sahu 2008; Scanlon and Kustas 2010, 2012). Comparisons in partitioning between E and T on monthly timescales will be used since there were frequent periods lacking convergence with the correlation-based flux partitioning method, but on a monthly time scale there were enough values to compare the partitioning of ET to T and E to significant changes in vine and interrow cover crop phenology. In general, this meant that both T and E contributions mainly came from the interrow cover crop during spring (March/April/early May) prior to and several weeks after bud break, during the fall (late September–November) after harvest, and possibly during winter season (December–February). Conversely, during the hot and dry summer months (June–August and early September) of the growing season, T mainly came from the vine canopy and E from the interrow (since cover crop over this period was senescent).

Approach

The TSEB model has undergone several modifications since it was first presented by Norman et al. (1995). Changes include refinements to the algorithm estimating soil aerodynamic resistance and shortwave and longwave transmittance through the canopy and addition of the Priestley–Taylor formulation for canopy transpiration (Kustas and Norman 1999). Further improvements include incorporating rigorous treatment of radiation modeling for strongly clumped row crops, accounting for shading effects on soil heat flux (Colaizzi et al. 2012a, 2016a, b), and incorporating alternative formulations for computing the canopy transpiration such as Penman–Monteith (PM) or light-use efficiency (LUE) parameterizations (see Colaizzi et al. 2012b, 2014, 2016c; Anderson et al. 2008).

Following a previous study in an olive orchard (Cammalleri et al. 2010), further refinements have been recently made to the within-canopy wind profile (Nieto et al. 2018a) to address the significant vertical variation in vine biomass which is often concentrated in the upper half of the canopy

with a secondary cover crop biomass in the interrow. This adjustment involved creating generic canopy profile distributions for four major seasonal/phenological stages. The first period is just before vine bud break when vine shoots are already pruned and there is an actively growing cover crop (March–April). The second period starts with vine bud break during the spring (April–May); at this time vine development is in the upper ~1/3 of the canopy between the first cordon where the vine shoots originate [~1.45 m above ground level (AGL)] and second trellis wire (~1.90 m AGL) used to support the vine shoots. The cover crop remains vigorous until it is mowed at the end of this period. In the third period, which includes the growing season through harvest as the vines undergo senescence (June–November), the foliage distribution is concentrated approximately midway between the ground and top of the vine canopy with no photosynthetic grass layer. Finally, a fourth distribution covers the period after vine leaf-off with standing vine shoots and a re-emerging cover crop (December–February).

Additionally, a simplified method to derive the clumping index for radiation modeling in vineyards was derived following the geometric model from Colaizzi et al. (2012a). A rectangular canopy shape, which simplifies the trigonometric calculations, replaces the elliptical hedgerow assumption in the original model. Results with this new modeling approach show similar accuracy to detailed three-dimensional radiation modeling schemes (Parry et al. this issue). A full description of the model formulations, modified and applied to the vineyard site using tower-based thermal measurements and aerial imagery, is provided in Nieto et al. (2018a, b). A description of the key TSEB model algorithms is provided in the Appendix 1 and also in Nieto et al. (2018a).

Materials and methods

The meteorological measurements were obtained from the flux towers located in the north (site 1) and south (site 2) vineyards (see Fig. 1). The vineyards are Pinot Noir (*Vitis vinifera*) variety with the north vineyard planted in 2009 and the south vineyard planted in 2011. Details of the flux tower measurements and post-processing of the raw 20 Hz data are described by Alfieri et al. (this issue). Daytime energy balance closure was on the order of 90% for both flux towers. Observed fluxes were corrected for closure errors using the residual method (i.e., assigning missing flux to ET) based on results from Kustas et al. (2015) using eddy covariance measurements in irrigated croplands under advection.

An overview of the post-processing of eddy covariance data can be found in Massman and Lee (2002). The correlation-based flux partitioning method has been described thoroughly in the literature (Scanlon and Sahu 2008; Scanlon

The measurements were collected in two vineyards located approximately
32 km (~20 mi) northeast of Lodi, CA (38.29°N, 121.12°W).

East-West Rows spaced ~3.3 m (11 ft). Vines spaced ~1.5 m (5 ft).

❖ North Vineyard (site 1):
 ➢ ~ 34.4 ha (85 ac).
 ➢ Planted in 2009.
❖ South Vineyard (site 2):
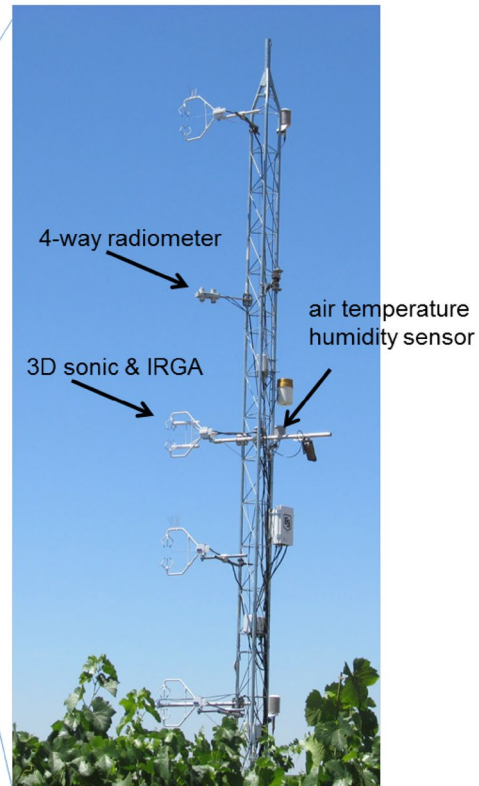 ➢ ~21 ha (52 acre).
 ➢ Planted in 2011.

Fig. 1 Description of study site and tower sensors used for running TSEB

and Kustas 2010; Palatella et al. 2014). The approach makes use of Monin–Obukhov similarity theory which implies that high-frequency time series for scalars, such as the water vapor (q) and carbon dioxide (c) concentrations, will yield perfect correlation when measured at the same point within the atmospheric surface layer. For q and c, one source/sink arises from the exchange of water vapor and carbon dioxide across leaf stomata during transpiration and photosynthesis, and a second from non-stomatal direct evaporation and respiration. If only T occurs, the similarity theory predicts a correlation of − 1 (a negative correlation because transpiration acts as a water vapor source and photosynthesis as a carbon sink). On the other hand, if only E occurs, the theory predicts a correlation of 1 (evaporation and respiration being sources for water vapor and carbon, respectively). Thus the q–c correlation will deviate from the expected − 1 correlation as E contribution increases or T/ET < 1. The premise of the correlation-based flux partitioning method technique is that an analysis of the degree of deviation from the expected − 1 correlation can be used to infer the relative amounts of T and E fluxes present.

In both 2014 and 2015, there was nearly a continuous set of high-frequency eddy covariance data available that allowed for estimates of monthly T/ET using the correlation-based flux partitioning eddy covariance (EC) method. Unfortunately, in 2016 there was a loss of the high-frequency data during the main growing season so it could not be used in this analysis. The model input data used in this study included 15-min wind speed measured at 5 m AGL from a three-dimensional sonic anemometer (CSAT3, Campbell Scientific, Logan, Utah USA[1]), air temperature from a Gill shielded temperature/humidity probe (HMP45C, Vaisala, Helsinki, Finland), and incoming radiation using a four-component net radiometer (CNR-1, Kipp and Zonen, Delft, Netherlands) mounted at 6 m AGL. The upwelling longwave radiation was used to compute a composite hemispherical LST (Norman and Becker 1995).

---

[1] The use of trade, firm, or corporation names in this article is for the information and convenience of the reader. Such use does not constitute official endorsement or approval by the US Department of Agriculture or the Agricultural Research Service of any product or service to the exclusion of others that may be suitable.

Other key inputs including canopy height, aerodynamic surface roughness, and leaf area index (LAI) were obtained from ground measurements during intensive observation periods (IOPs) which occurred during different key vine and cover crop phenological stages, namely April/May, June/July and August/September. However, the ground measurements required interpolation to daily values to run TSEB with the meteorological and LST inputs. For LAI, a machine learning approach (Gao et al. 2012) was applied to generate daily LAI maps at 30 m resolution over the GRAPEX field sites using Landsat surface reflectance and the MODIS LAI products. Agreement between the remotely sensed retrieved LAI and ground LAI measurements from 2013 to 2016 yielded an average difference of around 25% (Sun et al. 2017).

The remotely sensed LAI values do include the contribution of the cover crop in the interrow during periods of active transpiration and growth, which normally peaked in early spring and sometime after vine bud break. Daily canopy height was interpolated based on its relationship to LAI from Nieto et al. (2018a), and the aerodynamic roughness parameters were obtained from wind direction relative to vine row orientation (east–west rows) and their relationship to LAI derived by Alfieri et al. (this issue). Daily green vegetated fraction (f_G) used in the Priestley–Taylor formulation for canopy transpiration (see Nieto et al. 2018a) was estimated based on the day of year when senescence begins (DOY_S), which was observed from daily phenocam photos. $f_G = 1$ prior to DOY_S, then from DOY_S onward f_G follows a linearly decreasing function of LAI:

$$f_G(DOY > DOY_S)$$
$$= [(LAI(DOY)) - LAI_{min}] / [LAI(DOY_S) - LAI_{min}]. \tag{1}$$

Here, DOY is day of year and LAI_{min} is the estimated minimum annual value of LAI.

The value of the hemispherical LST (T_{RH}) can be computed based on the following expression:

$$T_{RH} = \left([R_{L\uparrow} - (1 - \varepsilon_H)R_{L\downarrow} + R_{Latm}] / \sigma\varepsilon_H \right)^{1/4}, \tag{2}$$

where $R_{L\uparrow}$ is the upwelling longwave radiation measurement, $R_{L\downarrow}$ is the downwelling longwave radiation, R_{Latm} is the atmospheric longwave contribution from ground to sensor height, σ is Stephan–Boltzmann constant and ε_H is the hemispherical emissivity estimated from weighting the fractional vegetation cover estimates (f_C) with assumed emissivity of the canopy (0.99) and soil/cover crop (0.94) as follows: $\varepsilon_H = 0.99(f_C) + 0.94(1 - f_C)$. Given the relatively small path length of the longwave sensor from the ground, it was assumed $R_{Latm} \sim 0$.

Results

For the years 2014–2016, the 15-min average meteorological and LST forcing data were used in TSEB along with daily LAI and aerodynamic roughness parameters to compute surface energy fluxes over the daytime period, which is defined when net radiation is greater than 100 W m^{-2}. The TSEB output for years 2014–2016 were computed. Since the focus is on ET and its partitioning between the vine canopy and the interrow, the model and measured results are compared using daytime ET and, when available, T/ET estimates using the correlation-based method with high-frequency eddy covariance data. As noted above, comparison of TSEB model estimates of T/ET with the correlation-based method was conducted on a monthly time scale and could only be carried out for years 2014 and 2015.

The daily daytime latent heat flux, LE or ET, sensible heat flux, H, net radiation, R_n, and soil heat flux, G, over the course of all 3 years for the north and south vineyards are illustrated in Fig. 2 using Eq. (1) to determine f_G. TSEB was also run using $f_G = 1$ over the full annual cycle for years 2014–2016; model results are similar with slightly greater bias. The figure indicates an overestimate in ET and an underestimate in H and only a slight bias in R_n and G for both vineyards.

The difference statistics with observed daytime ET (mm) and daytime H (MJ) for the different foliage distributions are listed in Table 1. Since the leaf-off and bud break statistical results were virtually the same, those two stages are combined in the table. The mean absolute percentage difference (MAPD) value, as defined in Table 1, was used as the key performance metric since it provides the relative magnitude of the observed flux to the model measurement difference. For the north vineyard, the performance of TSEB in LE is notably better over the growing season through senescence for all years while the spring or the leaf-off through bud break periods produced the greatest errors. However, for H difference statistics, the tendency was to have the largest errors during the growing season when ET is largest and H tends to be relatively small due to frequent irrigations combined with advection of heat from the surrounding mostly dry, arid region. For the south vineyard, MAPD values for LE estimation tended to be largest for leaf-off and bud break periods, which was also the case for H (except in 2016). Hence, for the south vineyard, it appears that the largest relative errors in ET for the different phenological stages are also associated with the greatest relative errors in H. This is not the case for the north vineyard.

The likely reason that the period of greatest errors (in terms of MAPD) in TSEB output for north and south vineyards differ stems from the fact that generally larger H values
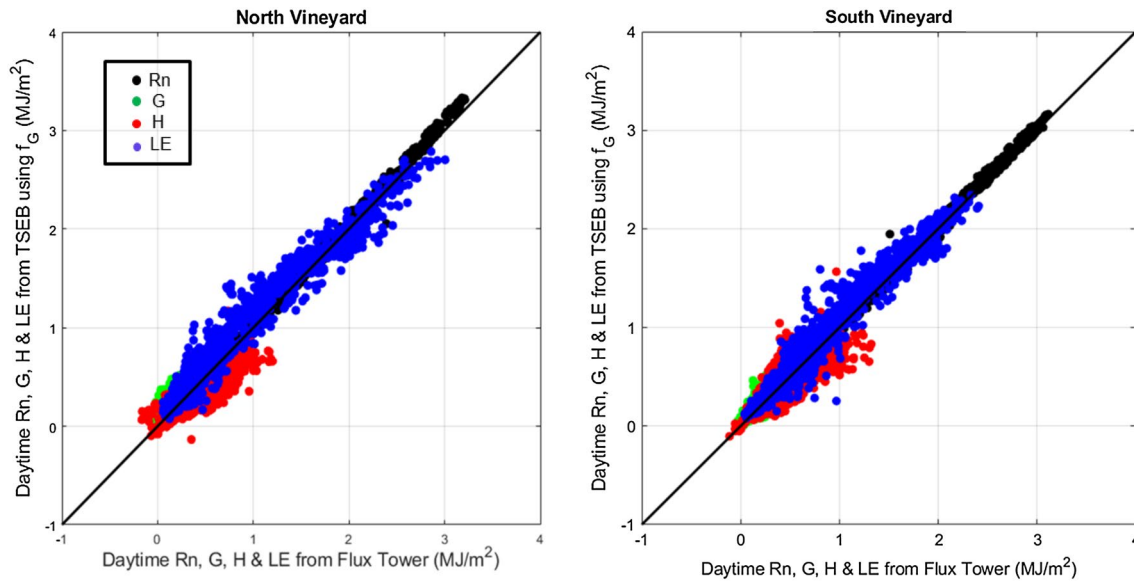
Fig. 2 Comparison of daytime net radiation (R_n), soil heat flux (G), sensible heat flux (H) and latent heat flux (LE) computed from hourly flux tower measurements from 2014 to 2016 for the north and south vineyards versus estimated from TSEB using f_G estimated from Eq. (1)

were measured for the south vineyard during the growing season due to lower biomass/leaf area and less irrigation (see below in the discussion of Fig. 6). It is evident from the yearly difference in Table 1 that in general, the TSEB model performs slightly better in the south vineyard than in the north, which agrees with the results from Nieto et al. (2018a). Slightly better model measurement agreement for the south vineyard may to some extent be due to greater variability in vine conditions in the north vineyard; this variability causes the T_{RH} observations to be generally less representative of the flux measurement footprint of thermal imagery source area (Knipper et al. this issue).

Figure 3 illustrates the effect of phenology-based f_G (Eq. 1) and temporal trend of LAI on the partitioning of LE between vine canopy or actively transpiring cover crop, and the interrow senescent cover crop/bare soil. The ratio of daytime vine/cover crop LE (LE$_C$ or T) in mm to total LE or ET are shown for both north and south vineyards for each of the three study years. As one would expect, the temporal trend in LE$_C$/LE or T/ET follows the temporal variations in LAI.

Early in the year, the cover crop is the primary contributor to T until it is mowed sometime in the middle of April (~DOY 100), usually soon after bud break. Then, LAI and T/ET increase as the vine canopy develops. By the end of June (~DOY 180), the vineyard phenology features transpiring vines and a fully senescent cover crop, and irrigation occurs every 2–3 days. Under these conditions one would expect T/ET near unity, but instead it decreases through the summer months as a result of the reduction of LAI through the veraison (July/early August, DOY 180–220) and harvest (late August/early September, DOY ~ 235–245) period. The

downward trend of T/ET is further amplified after the start of senescence in mid-September (DOY ~ DOY 260) due to the decreasing value of f_G. Due to the way that f_G is computed via Eq. (1) for each year, there is not a smooth transition in its value for year-to-year, namely $f_G < 1$ on December 31 (DOY 365) and then $f_G = 1$ on January 1 (DOY 1) the following year. This, however, does not cause a significant effect on the magnitude of T/ET since LAI is quite low over the winter months.

Figure 4 shows T/ET computed with TSEB and with the EC-based method for 2014 and 2015. In 2014, the T/ET of TSEB is decreasing (concave) during the main months of the growing season (June–August) while the EC-based method computes an increasing (convex) T/ET. A decreasing T/ET as the interrow cover crop undergoes senescence and the only source of water is from drip irrigation along the vine rows is contradictory both to what would be expected and to the EC method. However, the TSEB input of LAI from the remote sensing retrieval also shows a concave relationship over the main growing season (see Fig. 3), which is supported to some extent by the periodic ground measurements (Sun et al. 2017; White et al. this issue). However, the actual temporal behavior of LAI may not be totally consistent with the remote sensing method.

Additionally, in 2014, ground LAI observations along with the daily phenocam photos indicated the cover crop had re-emerged in July and August, which did not appear to affect the 30 m remotely sensed LAI product since the grass strips grew mainly along the borders of the vine row (see Fig. 5), but would have reduced the hemispherical LST values used as input to TSEB. This reduction in the magnitude

Table 1 Difference statistics between TSEB and measured daily daytime LE or ET (mm) and H (MJ/m²) for the different vine and cover crop phenological conditions

Difference statistics	2014 December–March	2014 April–May	2014 June–November	2015 December–March	2015 April–May	2015 June–November	2016 December–March	2016 April–May	2016 June–November	2014 Full year	2015 Full year	2016 Full year
	Leaf-off and bud break	Spring	Growing season and senescence	Leaf-off and bud break	Spring	Growing season and senescence	Leaf-off and bud break	Spring	Growing season and senescence			
North vineyard												
Evapotranspiration (ET)												
RMSD (mm)	0.25	0.44	**0.52**	0.37	**0.91**	0.35	0.39	**0.62**	0.56	0.42	0.6	0.53
Bias (mm)	0.08	**0.21**	0.12	0.18	**0.8**	−0.002	0.28	**0.55**	0.33	0.13	0.33	0.39
MAPD (%)	**21**	11	14	34	**42**	8	**40**	19	12	12	15	17
Sensible heat flux (H)												
RMSD (MJ)	0.1	0.17	**0.21**	0.1	0.14	**0.17**	0.06	0.18	**0.21**	0.17	0.14	0.16
Bias (MJ)	−0.03	−0.11	**−0.13**	0.003	−0.11	**−0.08**	−0.003	**−0.15**	−0.13	−0.1	−0.06	−0.09
MAPD (%)	27	24	**34**	26	21	**31**	18	30	**39**	24	25	27
South vineyard												
Evapotranspiration (ET)												
RMSD (mm)	0.3	0.31	**0.48**	0.31	**0.46**	**0.46**	0.26	**0.61**	0.46	0.37	0.41	0.46
Bias (mm)	0.04	0.11	**0.19**	0.02	0.1	**0.33**	0.14	**0.5**	0.28	0.12	0.15	0.31
MAPD (%)	**22**	9	12	**21**	12	11	18	**18**	**10**	12	13	14
Sensible heat flux (H)												
RMSD (MJ)	0.14	0.1	**0.16**	0.15	0.15	**0.21**	0.07	0.14	**0.2**	0.13	0.17	0.15
Bias (MJ)	0.07	0.04	**−0.1**	0.07	0.004	**−0.17**	0.03	−0.11	**−0.15**	0.002	−0.03	−0.08
MAPD (%)	**37**	14	27	**39**	15	26	23	21	**30**	23	24	25

Numbers in bold indicate largest difference statistic computed in each year

RMSD = sqrt[average[(model − observed)²]]

MAPD = 100 × [average[absolute(model − observed)]/average(observed)]

BIAS = average[model − observed]

of LST in turn would likely have increased the interrow E contribution estimated by TSEB (since remotely sensed LAI of the vines did not change or actually decreased according to Fig. 3) relative to T from the vines. On the other hand, the EC-based method would have added the cover crop T contribution with the vine T, increasing the overall T/ET ratio.

Better agreement between TSEB-derived T/ET (LE_C/LE) monthly values and the EC method is observed for 2015 versus 2014, particularly for the north vineyard. Additionally, the agreement appears quite good during the senescent periods (October–February) and through bud break and flowering (March–May). This is particularly true in 2015 for the north vineyard. Since much of the cover crop is senescent by end of June (DOY ~ 180), one might expect T/ET to peak in July–August, which is what the estimates using the correlation-based flux partitioning method appear to show. This result needs to be tested with other independent measurements of vine transpiration and interrow cover crop and soil evaporation measurements. However, a major issue with using localized measurements of LST and LAI is the lack of representativeness in relation to the flux tower measurement source area footprint.

In 2015, a set of interrow flux observations was collected using micro-Bowen ratio systems in the north vineyard described in Kustas et al. (this issue). The Bowen ratio, H/LE, is another way to express surface energy partitioning. There were three micro-Bowen ratio (MBR) systems deployed in the interrow of the north vineyard within the footprint of the flux tower using the sensor design of Holland et al. (2013). One MBR system was in the center of the interrow, another under the north facing vine row and a third in the south facing vine row. There are only a handful of reliable measurements available during the four intensive observation periods (IOPs). These were collected on DOY 113, 153, 192 and 224 which are late April (IOP 1) soon after bud break, early June (IOP 2) near maximum LAI, mid-July (IOP 3) around the berry setting stage, and mid-August (IOP 4) well into the veraison stage along with cane/vine maturation. Estimates of the T/ET ratio for these days were computed using the eddy covariance measurements of the total ET along with the micro-Bowen ratio estimates from the interrow comprising E from the bare soil areas and ET or E from the cover crop, which make up approximately 40% and 60% of the interrow, respectively. The estimated daily ratios of T/ET are compared with the TSEB estimates in Fig. 6.

For IOP 1, TSEB gives a higher T/ET than the micro-Bowen ratio estimate, where T and ET are mainly from the cover crop, while for IOP 2 and 3 the agreement in the T/ET partitioning is very good. However, for IOP 4 in August, the T/ET ratio from TSEB is lower than estimated by the EC flux tower/micro-BR system. The results for IOP 1 and 4 are consistent with the monthly T/ET comparison in Fig. 4 for the north vineyard in 2015.

Figure 7 illustrates the difference in energy balance between the vine and interrow by way of the evaporative fraction (EF = LE/(H + LE)) of the vine/cover crop EF_C = LE_C/(H_C + LE_C) and the interrow bare soil/substrate EF_S = LE_S/(H_S + LE_S). Also plotted are the precipitation and irrigation events and amounts in mm and mm/vine, respectively. As expected, under these mostly well-watered conditions, EF_C is near unity except during the period of leaf off through bud break, nominally the period DOY < 100 and DOY > 275, January–April and October–December, respectively. Main vine growth and berry development, concurrent with the majority of vineyard irrigation, occur from nominally DOY 125 through DOY 250, May–September.

Values of EF_S tend to be lowest (EF_S < 0.5) just prior to bud break (~ DOY 100, early April) and highest (closer to 1) after leaf off, nominally DOY > 275, early October. The low EF_S values prior to bud break may be due to the re-emergence of the cover crop, while the higher values in EF_S are likely due to irrigation after harvest and leaf off as well as winter precipitation during the senescence of both vines and cover crop. Depending on the year, the values of EF_S during the main vine and berry growth and development period, roughly DOY 100–250 (April–early September), lie between 0.25 and 0.75. However, one would expect for EF_S values to generally be well below 0.5 during the main part of the growing season since EF_S = 0.5 is equivalent to a Bowen ratio of order 1, or equal partitioning into H and LE. There are generally lower values of EF_S for the south vineyard in 2015, which coincides with noticeably lower irrigation amounts; this trend is also evident to some extent in 2016. Therefore, it may be that the frequent irrigations lead to higher than expected EF_S values in the summer months; however, it also appears the TSEB formulation may not always properly partition E and T, particularly late in the growing season.

Lastly, due to the method for computing f_G via Eq. (1), as described earlier, the transition from year-to-year is abrupt from f_G < 1 to f_G = 1. Although this did not have a major impact on T/ET ratio, it does cause a significant change in EF_C. For example, the value of EF_C changes from ~ 0.25 on December 31 (DOY 365) 2014 to EF_C ~ 0.75 on January 1 (DOY 1) 2015. A different formulation is under development and will be applied over the winter months such that for multi-year model runs this inconsistency in f_G for consecutive years is mitigated.

Summary and conclusions

Using hemispherical land surface temperature from tower upwelling longwave observations from 2014 to 2016, the TSEB model was run over all seasons with available data
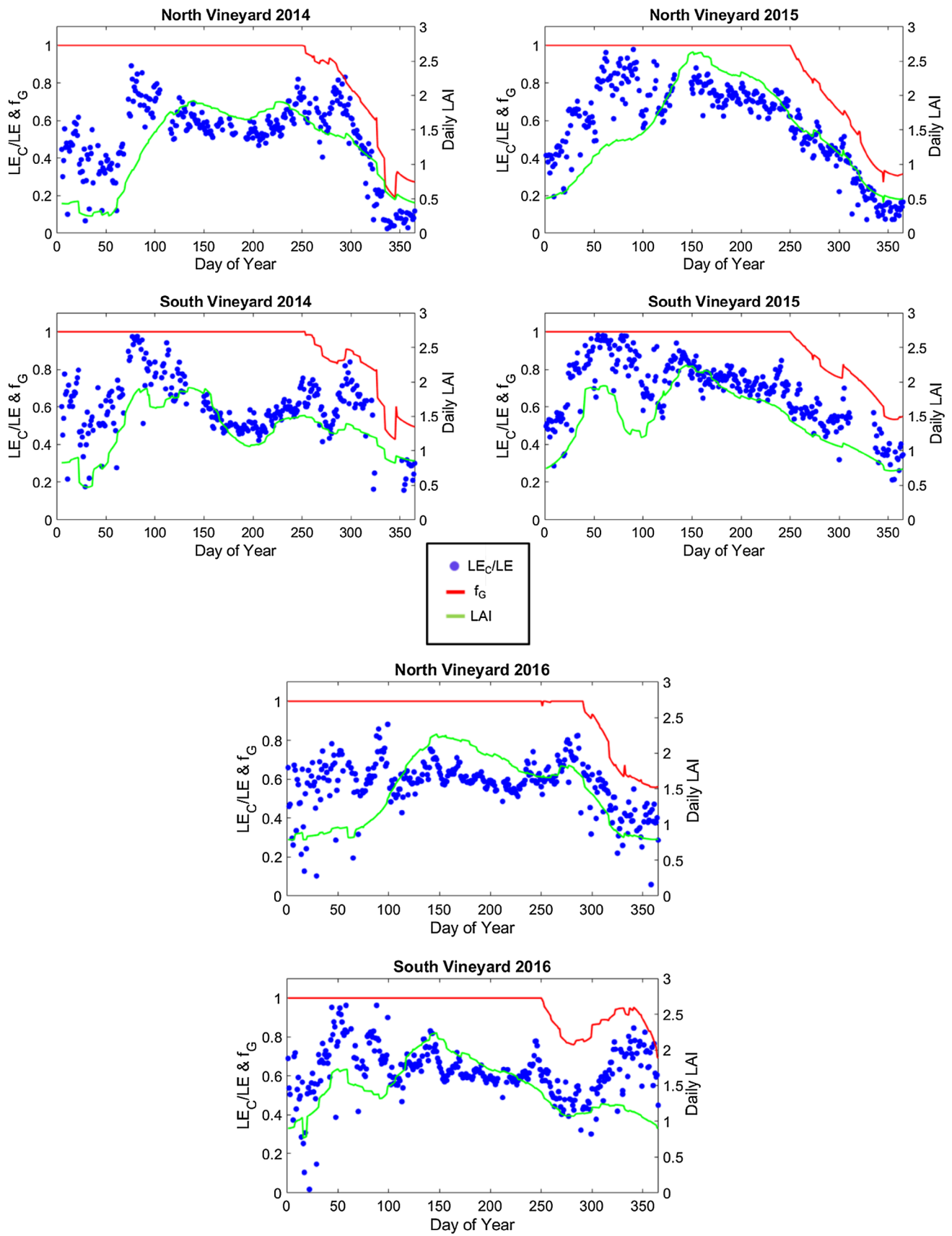
◄**Fig. 3** Daytime values of the ratio LE$_C$/LE or T/ET estimated from TSEB for 2014–2016 using f_G estimated from Eq. (1) and daily LAI from remote sensing retrievals

to compute surface energy fluxes with a focus on estimating daytime ET. Several of the original TSEB formulations of radiation and wind extinction through the vine canopy layer were modified based on the results of Nieto et al. (2018a, b). The resulting agreement between TSEB-estimated daytime sensible (H) and latent heat (LE) fluxes and flux tower observations indicated that for the north vineyard, the largest relative differences (MAPD values) in LE occurred in either the spring or during leaf-off and bud break periods. For H the largest MAPD values for the north vineyard occurred during the growing and senescent periods. For the south vineyard, the largest MAPD values for LE and for H were also from the leaf-off and bud break periods. The only exception to this was in 2016 when the largest MAPD value for H was during the growing season and senescent period. Since the south vineyard had less-irrigated vine biomass, H was generally larger over the growing season, making relative errors smaller.

The TSEB model estimates the daytime source of LE or ET during the growing season is 50–70% from the vine canopy in 2014 and 70–80% in 2015. For 2014, the TSEB-derived T/ET is in poor agreement with the correlation-based flux partitioning method which estimated T/ET of 80–90% during the growing season while there is much closer agreement in T/ET for 2015. The poor performance in 2014 partitioning may be due in part to a reduction of LAI estimated by the remote sensing method (Fig. 3) combined with re-emergence of the cover crop mainly along the vine row (Fig. 5) not detected by satellite, but likely reducing the magnitude of the LST observations. Without an increase in LAI, this in turn is likely to cause TSEB to increase the E contribution from the interrow. During periods of no or insignificant vine biomass, the transpiring interrow cover crop and bare soil mainly contributes to ET. Evaluation of the partitioning between soil and vegetation sources of LE shows that LE$_C$/LE or T/ET ratio starts around a value of 1 (100%) in early spring when the cover crop is rapidly growing and transpiring, decreases after cover crop mowing, increases again from bud break until peak LAI, gradually declines through harvest, and finally increases in late autumn as the cover crop rebounds. This partitioning between E and T is controlled in large part by the remotely sensed LAI estimates, which generally indicated a peak LAI in late May/early June followed by a gradual decline over the course of the growing season (see Fig. 3).

In 2015, on selected days during the IOPs there were T/ET estimates using micro-Bowen ratio measurements of E and ET components for the interrow cover crop and bare

soil together with total ET from the flux towers. The agreement in the T/ET ratios was good for IOPs 2 and 3, which were early June and mid-July, but over and underestimated for IOPs 1 and 4 in late April and mid-August, respectively. The results for IOPs 1 and 4 are consistent with the monthly T/ET TSEB versus EC method comparisons.

The partitioning ratios of LE$_C$/LE or T/ET for the interrow cover crop/bare soil and vine canopy, calculated by TSEB, tend to be higher than the values from the correlation-based flux partitioning EC method during the leaf-off and bud break periods but lower than the EC method values during the growing season through senescence. This temporal trend in T/ET partitioning estimated from TSEB is significantly affected by the temporal trend in LAI, which from the remote sensing method generally shows an increase in LAI in response to growth of the cover crop in the spring followed by a decline after cover crop mowing, and then an increase after vine bud break in March until end of May/early June. This behavior is followed by a general decline over the growing season as the cover crop undergoes senescence and the vines are managed/pruned. Then after harvest the trend in T/ET continues to decrease as the vines are dormant and cover crop recovers slowly during the winter rains and cooler temperatures.

The magnitude of the evaporative fraction of the soil/substrate (EF$_S$) estimated by TSEB is generally scattered around 0.5 ($\pm$0.25) during the growing season; EF$_S$ = 0.5 indicates a Bowen ratio of 1, or equal partitioning of the available energy between H and LE. This LE$_S$ component seems too large for the underlying non-irrigated senescent cover crop interrow, albeit approximately 40% of the interrow is composed of irrigated bare soil. The response of higher EF$_S$ values for the north vineyard, which tended to receive higher irrigation amounts, is plausible. However, one would still not expect EF$_S$ values to exceed 0.5.

Clearly, more detailed measurements are needed to better determine whether the errors in partitioning are the result of biases or errors in the inputs to TSEB, principally in estimates of the leaf area and hemispherical land surface temperature. This study should include applying several methods for estimating the partitioning of ET into vine transpiration using sapflow gages and perhaps microlysimeters as well as more detailed below canopy measurements following the below canopy measurement design of Kool et al. (2016) for estimating E and when appropriate T contributions from the interrow.

Reliable estimates of vine transpiration relative to the total ET is valuable information for determining vine water use and stress, both of which influence grape yield and quality. This need has led others to develop crop water stress indices using very high-resolution aerial thermal imagery to define vine-only stress and water potential for irrigation scheduling (Bellvert et al. 2016). With coarser resolution
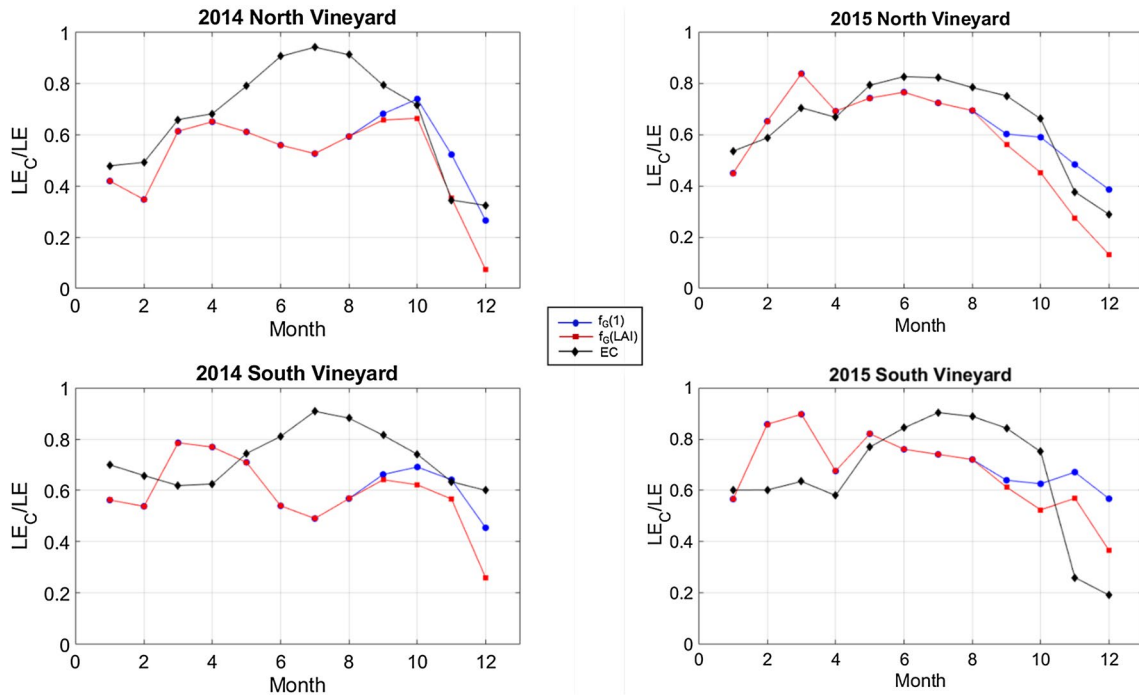
Fig. 4 The monthly average values of LE_C/LE or T/ET estimated from TSEB for 2014 and 2015 using $f_G(LAI)$: f_G estimated from Eq. (1), $f_G(1)$: assuming $f_G = 1$ all year, and EC: estimated using the correlation-based flux partitioning method

Fig. 5 Phenocam photo in north vineyard during IOP 4 in early August, 2014

thermal imagery routinely available from satellites (Semmens et al. 2016; Knipper et al. this issue), reliable partitioning of ET into T and E, particularly during the vine growing season, could be used to define a stress index which could relate to the crop/vine water stress index and lead to estimating leaf/vine water potential for irrigation scheduling at the field scale.
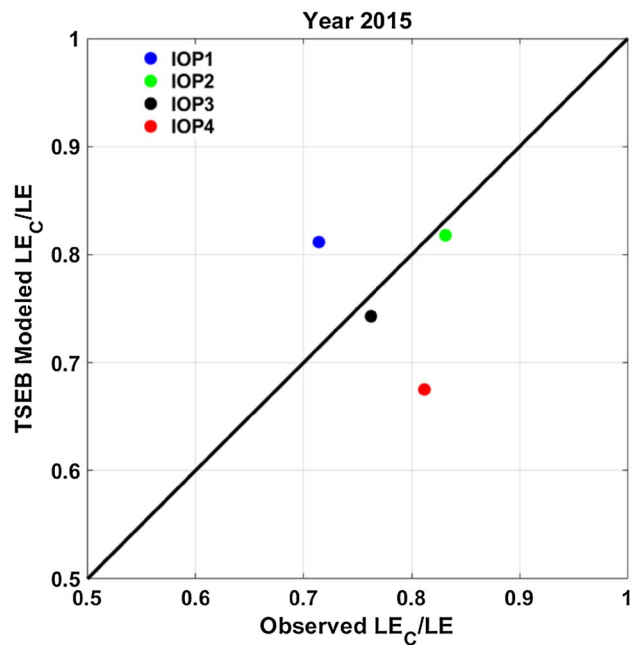
Fig. 6 Comparison of TSEB model estimated daytime LE_C/LE using f_G estimated from Eq. (1) versus observed ratio for each of the four IOPs in 2015 (IOP 1 = late April; IOP 2 = early June; IOP 3 = mid-July; IOP 4 = late August) using the tower ET and micro-Bowen ratio measurements of bare soil and cover crop interrow LE and LE_C from the north vineyard (see Kustas et al. this issue)
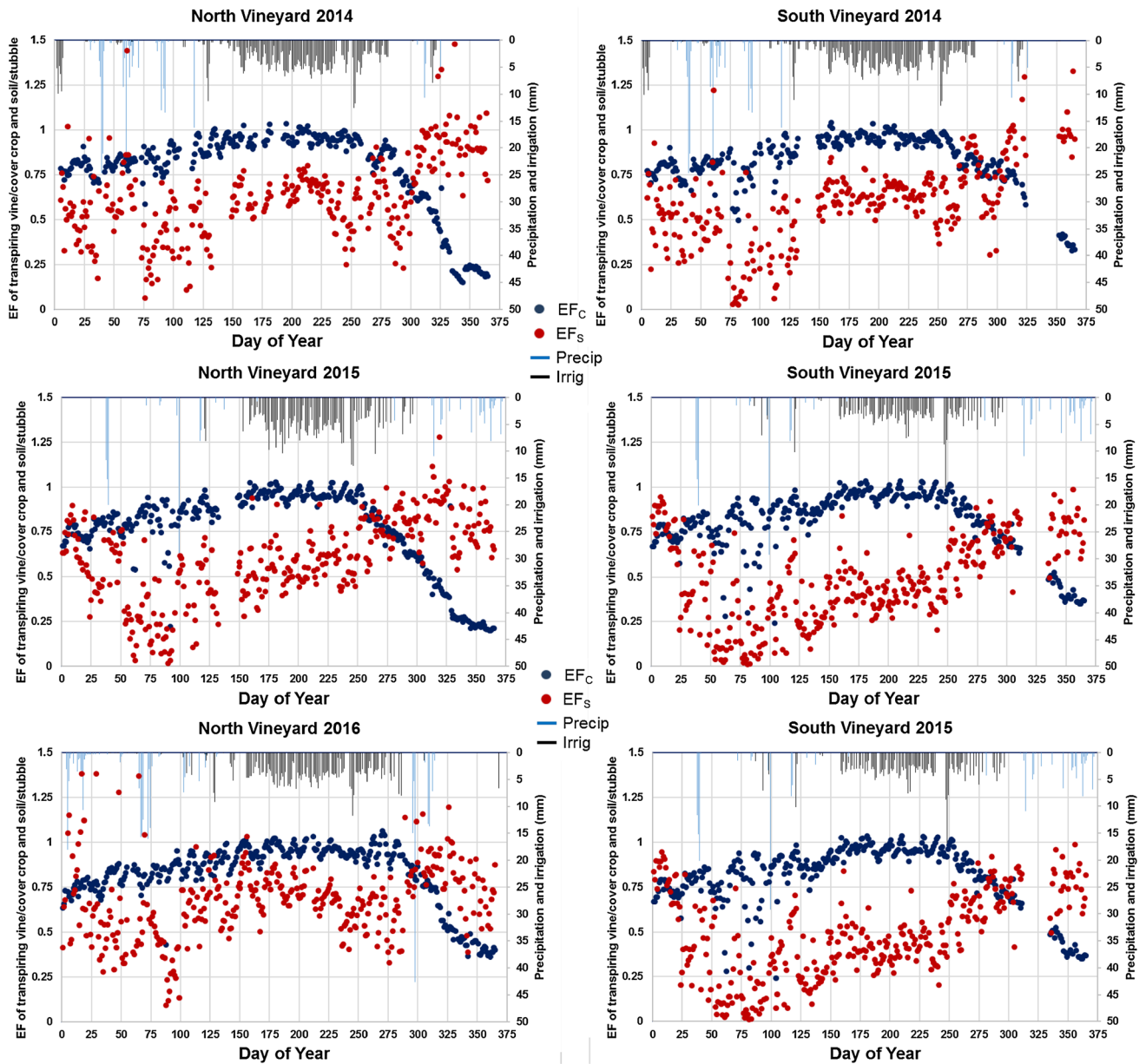
Fig. 7 Evaporative fraction (EF) calculated using the TSEB model for the vine/cover crop (EF_C) and the interrow bare soil/senescent cover crop (EF_S)

Compliance with ethical standards

Conflict of interest On behalf of all authors, the corresponding author states that there is no conflict of interest.

Appendix 1: TSEB model

The basic equation of the energy balance at the surface can be expressed following Eq. (3).

$$R_n \approx H + LE + G$$
$$R_{n,S} \approx H_S + LE_S + G$$
$$R_{n,C} \approx H_C + LE_C \quad (3)$$

with R_n being the net radiation, H the sensible heat flux, LE the latent heat flux or evapotranspiration, and G the soil heat flux. "C" and "S" subscripts refer to canopy and soil layers respectively. The symbol "$\approx$" appears since there are additional components of the energy balance that are usually neglected, such as heat advection, storage of energy in the canopy layer or energy for the fixation of CO_2 (Hillel 1998).

The key in TSEB models is the partition of sensible heat flux into the canopy and soil layers, which depends on the soil and canopy temperatures (T_S and T_C, respectively). If we assume that there is an interaction between the fluxes of canopy and soil, due to an expected heating of the in-canopy air by heat transport coming from the soil, the resistances network in TSEB is considered in series. In that case H can be estimated as in Eq. (4) [Norman et al. 1995, Eqs. (A.1)–(A.4)]

$$H = H_C + H_S = \rho_{air} C_p \frac{T_{AC} - T_A}{R_a}$$
$$= \rho_{air} C_p \left[\frac{T_C - T_{AC}}{R_x} + \frac{T_S - T_{AC}}{R_s} \right], \quad (4)$$

where ρ_{air} is the density of air (kg m^{-3}), C_p is the heat capacity of air at constant pressure (J kg^{-1} K^{-1}), T_{AC} is the air temperature at the canopy interface (K), equivalent to the aerodynamic temperature T_0, computed as follows (Norman et al. 1995, Eq. A.4):

$$T_{AC} = \frac{\frac{T_A}{R_a} + \frac{T_C}{R_x} + \frac{T_S}{R_s}}{\frac{1}{R_a} + \frac{1}{R_x} + \frac{1}{R_s}}. \quad (5)$$

Here, R_a is the aerodynamic resistance to heat transport (s m^{-1}), R_s is the resistance to heat flow in the boundary layer immediately above the soil surface (s m^{-1}), and R_x is the boundary layer resistance of the canopy of leaves (s m^{-1}). The mathematical expressions of these resistances are detailed in Norman et al. (1995) and Kustas and Norman (2000), discussed in Kustas et al. (2016), and shown below:

$$R_a = \frac{\ln\left(\frac{z_T - d_0}{z_{0H}}\right) - \Psi_h\left(\frac{z_T - d_0}{L}\right) + \Psi_h\left(\frac{z_{0H}}{L}\right)}{\kappa' u_*}$$
$$R_s = \frac{1}{c\left(T_S - T_A\right)^{1/3} + bu_s}$$
$$R_x = \frac{C'}{LAI}\left(\frac{l_w}{U_{d_0 + z_{0M}}}\right)^{1/2}, \quad (6)$$

where u_* is the friction velocity (m s^{-1}) computed as:

$$u_* = \frac{\kappa' u}{\left[\ln\left(\frac{z_u - d_0}{z_{0M}}\right) - \Psi_m\left(\frac{z_u - d_0}{L}\right) + \Psi_m\left(\frac{z_{0M}}{L}\right)\right]}. \quad (7)$$

In Eq. (7), z_u and z_T are the measurement heights for wind speed u (m s^{-1}) and air temperature T_A (K), respectively. d_0 is the zero-plane displacement height, z_{0M} and z_{0H} are the roughness length for momentum and heat transport respectively (all those magnitudes expressed in m), with $z_{0H} = z_{0M}\exp(-kB^{-1})$. In the series version of TSEB z_{0H} is assumed to be equal to z_{0M} since the term R_x already accounts for the different efficiency between heat and momentum transport (Norman et al. 1995), and therefore $kB^{-1} = 0$. The value of $\kappa' = 0.4$ is the von Karman's constant. The Ψ_m and Ψ_h terms in Eqs. (6) and (7) are the adiabatic correction factors for momentum and heat, respectively, whose formulations are described in Brutsaert (1999, 2005) and are functions of the atmospheric stability. The stability is expressed using the Monin–Obukhov length L (m), which has the following form:

$$L = \frac{-u_*^3 \rho_{air}}{kg\left[H/\left(T_A C_p\right) + 0.61E\right]}, \quad (8)$$

where H is the bulk sensible heat flux (W m^{-2}), E is the rate of surface evaporation (kg s^{-1}), and g the acceleration of gravity (m s^{-2}).

The coefficients b and c in Eq. (6) depend on turbulent length scale in the canopy, soil surface roughness and turbulence intensity in the canopy, which are discussed in Sauer et al. (1995), Kondo and Ishida (1997) and Kustas et al. (2016). C' is assumed to be 90 s$^{1/2}$ m^{-1} and l_w is the average leaf width (m).

Wind speed at the heat source sink ($z_{0M} + d_0$) and near the soil surface was originally estimated in TSEB using the Goudriaan (1977) wind attenuation model:

$$U(z) = U_C \exp\left[-a_G\left(1 - z/h_c\right)\right]$$
$$a_G = 0.28 LAI^{2/3} h_c^{1/3} l_w^{-1/3}. \quad (9)$$

For the vineyards, Nieto et al. (2018a) utilized a new wind profile formulation developed by Massman et al. (2017). This canopy wind profile model is a more physically based method for calculating wind speed attenuation for the canopies of vertically non-uniform foliage distribution and leaf area that often exist in orchards and vineyards.

When only a single observation of T_{rad} is available (i.e., measurement at a single angle), partitioning of T_{rad} into canopy and soil components (T_C and T_S) is required to estimate component sensible heat fluxes via Eq. (4). The approach developed for TSEB (Norman et al. 1995) starts with an

initial estimate of plant transpiration (LE_C), as defined by the Priestley and Taylor (1972) relationship, applied to the canopy divergence of net radiation ($R_{n,C}$)

$$LE_C = \alpha_{PT} f_g \frac{\Delta}{\Delta + \gamma} R_{n,C}. \tag{10}$$

Here, α_{PT} is the Priestley–Taylor coefficient, initially set to 1.26, f_g is the fraction of vegetation that is green and hence capable of transpiring, Δ is the slope of the saturation vapor pressure versus temperature curve, and γ is the psychrometric constant. This method allows the canopy sensible heat flux to be calculated using the energy balance at the canopy layer ($H_c = R_{n,C} - LE_C$) and hence an estimate of T_C to be obtained by rewriting Eq. 10 to have the following form (Norman et al. 1995):

$$T_{Ci} = T_a + \frac{R_{n,C} R_a}{\rho C_p} \left[1 - \alpha_{PT} f_G \frac{\Delta}{\Delta + \gamma} \right], \tag{11}$$

where T_{Ci} is the initial estimate of canopy temperature. Alternatively, T_{Ci} can be derived with the linearization approximation to the series resistance approach described in Appendix A of Norman et al. (1995), specifically Eqs. (A.10)–(A.13). Then, T_S is the derived from the following using T_{rad}, T_C, and an estimate of $f_c(\theta)$, the fraction of vegetation observed by the sensor view zenith angle θ:

$$T_{rad}^4(\theta) = f_c(\theta) T_C^4 + \left[1 - f_c(\theta) \right] T_S^4. \tag{12}$$

The value of $f_c(\theta)$ is typically estimated as an exponential function of the leaf area index (LAI), which includes a clumping factor or index Ω for canopies where the LAI is concentrated for sparsely distributed plants or for organized canopies such as row crops (Kustas and Norman 1999; Anderson et al. 2005), and has the following form:

$$f_c(\theta) = 1 - \exp\left(\frac{-0.5\Omega LAI}{\cos\theta} \right). \tag{13}$$

However, due to the unique vertical canopy structure and wide row width relative to canopy height of vineyards, a new method to derive Ω had to be developed that was both based on the geometric model of Colaizzi et al. (2012a) and simple enough to be incorporated into TSEB. Parry et al. (this issue) compared radiation extinction models of different complexities and found the simplified geometric model developed by Nieto et al. (2018b) was a robust modified radiation scheme. The resulting effective LAI, $LAI_{eff} = \Omega LAI$, was then used as input in the Campbell and Norman (1998) canopy radiative transfer model to estimate soil and canopy net radiation, $R_{n,S}$ and $R_{n,C}$, respectively (see also Kustas and Norman 2000 for details).

The final energy balance component of soil heat flux, G, is typically estimated by TSEB as a fraction of the net radiation at the soil surface, $R_{n,S}$. However, over the daytime period, the assumption of a constant ratio between G and $R_{n,S}$ is unreliable (Santanello and Friedl 2003; Colaizzi et al. 2016a, b). Based on observations between the measured soil heat flux and the estimated $R_{n,S}$ in Nieto et al. (2018b), a modified formulation estimating G as a function of $R_{n,S}$ was adopted that accounts for the temporal behavior of the $G/R_{n,S}$ ratio over the daytime period using a double asymmetric sigmoid function; this estimate was a significantly better fit to the observations than the sinusoidal function proposed by Santanello and Friedl (2003).

With $R_{n,S}$ and G estimated and H_S computed via T_S estimated from Eqs. (11)–(13), iteratively solving for Eqs. (4)–(9) results in LE_s solved as a residual via Eq. (3) for the soil layer, namely $LE_s = R_{n,S} - G - H_S$.

In some cases, the initial T_C implied by the Priestley–Taylor approximation (Eq. 11) results in deriving a relatively high value of T_S for a given observed T_{rad} and $f_c(\theta)$ condition. This high T_S can cause a significant overestimate in H_S and therefore produce unrealistic estimates of LE_S (i.e., negative values during daytime; $LE_s < 0$) solved by residual. In this case, the α_{PT} coefficient is iteratively reduced at 0.1 intervals from its initial value ~ 1.26, effectively assuming the canopy is stressed and transpiring at sub-potential levels until $LE_s \geq 0$.

References

Alfieri JG, Kustas WP, Prueger JH, McKee LG, Hipps LE, Gao F (this issue) A multi-year intercomparison of micrometeorological observations at adjacent vineyards in California's central valley during GRAPEX. Irrig Sci

Anderson MC, Norman JM, Kustas WP, Li F, Prueger JH, Mecikalski JR (2005) Effects of vegetation clumping on two–source model estimates of surface energy fluxes from an agricultural landscape during SMACEX. J Hydromet 6(6):892–909

Anderson MC, Norman JM, Kustas WP, Houborg JM, Starks PJ, Agam N (2008) thermal-based remote sensing technique for routine mapping of land-surface carbon, water and energy fluxes from field to regional scales. Remote Sens Environ 112:4227–4241

Bellvert J, Zarco-Tejada P, Marsal J, Girona J, Gonzalez-Dugo V, Fereres E (2016) Vineyard irrigation scheduling based on airborne thermal imagery and water potential thresholds. Aust J Grape Wine Res 22(2):307–315. https://doi.org/10.1111/ajgw.12173

Brutsaert W (1999) Aspects of bulk atmospheric boundary layer similarity under free-convective conditions. Rev Geophys 37(4):439–451

Brutsaert W (2005) Hydrology. An introduction. Cambridge University Press, Cambridge (ISBN-13 978-0-521-82479-8)

Cammalleri C, Anderson MC, Ciraolo G, D'Urso G, Kustas WP, La Loggia G, Minacapilli M (2010) The impact of in-canopy wind profile formulations on heat flux estimation in an open orchard using the remote sensing-based two-source model. Hydrol Earth Sys Sci 14(12):2643–2659

Campbell GS, Norman JM (1998) An introduction to environmental biophysics, 2nd edn. Springer, New York

Colaizzi PD, Evett SR, Howell TA, Li F, Kustas WP, Anderson MC (2012a) Radiation model for row crops: I. Geometric view factors and parameter optimization. Agron J 104:225–240

Colaizzi PD, Kustas WP, Anderson MC, Agam N, Tolk JA, Evett SR, Howell TA, Gowda PH, O'Shaughnessy SA (2012b) Two-source energy balance model estimates of evapotranspiration using component and composite surface temperatures. Adv Water Resour 50:134–151

Colaizzi PD, Agam N, Tolk JA, Evett SR, Howell TA, Gowda PH, O'Shaughnessy SA, Kustas WP, Anderson MC (2014) Two-source energy balance model to calculate E, T, and ET: comparison of Priestley–Taylor and Penman–Monteith formulations and two time scaling methods. Trans ASABE 57(2):479–498

Colaizzi PD, Evett SR, Agam N, Schwartz RC, Kustas WP (2016a) Soil heat flux calculation for sunlit and shaded surfaces under row crops: 1. Model development and sensitivity analysis. Agric For Meteorol 216:115–128

Colaizzi PD, Evett SR, Agam N, Schwartz RC, Kustas WP, Cosh MH, McKee LG (2016b) Soil heat flux calculation for sunlit and shaded surfaces under row crops: 2. Model test. Agric For Meteorol 216:129–140

Colaizzi PD, Agam N, Tolk JA, Evett SR, Howell TA, O'Shaughnessy SA, Gowda PH, Kustas WP, Anderson MC (2016c) Advances in a two-source energy balance model: partitioning of evaporation and transpiration for cotton using component and composite surface temperatures. Trans ASABE 59(1):181–197. https://doi.org/10.13031/trans.59.11215

Gao F, Anderson MC, Kustas WP, Wang Y (2012) A simple method for retrieving leaf area index from landsat using MODIS LAI products as reference. J Appl Remote Sens. https://doi.org/10.1117/.JRS.1116.063554

Goudriaan J (1977) Crop micrometeorology: a simulation stud. Tech. rep. Center for Agricultural Publications and Documentation, Wageningen

Hillel D (1998) Environmental soil physics. Academic Press, New York

Holland S, Heitman JL, Howard A, Sauer TJ, Giese W, Ben-Gal A, Agam N, Kool D, Havlin J (2013) Micro-Bowen ratio system for measuring evapotranspiration in a vineyard interrow. Agric For Meteorol 177:93–100

Knipper KR, Kustas WP, Anderson MC, Aleri JG, Prueger JH, Hain CR, Gao F, Yang Y, McKee LG, Nieto H, Hipps LE, Alsina MM, Sanchez L (this issue) Evapotranspiration estimates derived using thermal-based satellite remote sensing and data fusion for irrigation management in California vineyards. Irrig Sci

Kondo J, Ishida S (1997) Sensible heat flux from the earth's surface under natural convective conditions. J Atmos Sci 54(4):498–509

Kool D, Agam N, Lazarovitch N, Heitman JL, Sauer TJ, Ben-Gal A (2014) A review of approaches for evapotranspiration partitioning. Agric For Meteorol 184:56–70

Kool D, Kustas WP, Ben-Gal A, Lazarovitch N, Heitman JL, Sauer TJ, Agam N (2016) Energy and evapotranspiration partitioning in a desert vineyard. Agric For Meteorol 218–219:277–287

Kustas WP, Norman JM (1999) Evaluation of soil and vegetation heat flux predictions using a simple two-source model with radiometric temperatures for partial canopy cover. Agric For Meteorol 94:13–29

Kustas W, Norman JM (2000) A two-source energy balance approach using directional radiometric temperature observations for sparse canopy covered surfaces. Agron J 92(5):847–854

Kustas WP, Alfieri JG, Agam N, Evett SR (2015) Reliable estimation of water use at field scale in an irrigated agricultural region with strong advection. Irrig Sci 33:325–338

Kustas WP, Nieto H, Morillas L, Anderson MC, Alfieri JG, Hipps LE, Villagarcía L, Domingo F, García M (2016) Revisiting the paper "using radiometric surface temperature for surface energy flux estimation in mediterranean drylands from a two-source perspective. Remote Sens Environ 184:645–653

Kustas WP, Agam N, Alfieri AJ, McKee LG, Preuger JH, Hipps LE, Howard AM, Heitman JL (this issue) Below canopy radiation divergence in a vineyard—implications on inter-row surface energy balance. Irrig Sci

Massman WJ, Lee X (2002) Eddy covariance flux corrections and uncertainties in long term studies of carbon and energy exchanges. Agric For Meteorol 113:121–144

Massman W, Forthofer J, Finney M (2017) An improved canopy wind model for predicting wind adjustment factors and wildland fire behavior. Can J For Res 47(5):594–603

Nieto H, Kustas W, Gao F, Alfieri J, Torres A, Hipps L (2018a) Impact of different within-canopy wind attenuation formulations on modelling sensible heat flux using TSEB. Irrig Sci. https://doi.org/10.1007/s00271-018-0611-y

Nieto H, Kustas WP, Torres-Rúa A, Alfieri JG, Gao F, Anderson MC, White WA, Song L, del Mar Alsina M, Prueger JH, McKee M, Elarab M, McKee LG (2018b) Evaluation of TSEB turbulent fluxes using different methods for the retrieval of soil and canopy component temperatures from UAV thermal and multispectral imagery. Irrig Sci. https://doi.org/10.1007/s00271-018-0585-9

Norman JM, Becker F (1995) Terminology in thermal infrared remote sensing of natural surfaces. Remote Sens Rev 12:159 – 173

Norman JM, Kustas WP, Humes KS (1995) Source approach for estimating soil and vegetation energy fluxes in observations of directional radiometric surface temperature. Agric Fort Meteorol 77(3–4):263–293

Palatella L, Rana G, Vitale D (2014) Towards a flux-partitioning procedure based on the direct use of high-frequency eddy-covariance data. Bound Layer Meteorol 153:327–337

Parry CK, Nieto H, Guillevic P, Agam N, Kustas WP, Alfieri J, McKee L, McElrone AJ (this issue) An intercomparison of radiation partitioning models in vineyard row structured canopies. Irrig Sci

Priestley CHB, Taylor RJ (1972) On the assessment of surface heat flux and evaporation using large-scale parameters. Mon Weather Rev 100(2):81–92

Santanello J Jr, Friedl M (2003) Diurnal covariation in soil heat flux and net radiation. J Appl Meteorol 42(6):851–862

Sauer TJ, Norman JM, Tanner CB, Wilson TB (1995) Measurement of heat and vapor transfer coefficients at the soil surface beneath a maize canopy using source plates. Agric Fort Meteorol 75(1–3):161–189

Scanlon TM, Kustas WP (2010) Partitioning carbon dioxide and water vapor fluxes using correlation analysis. Agric For Meteorol 150:89–99

Scanlon TM, Kustas WP (2012) Partitioning evapotranspiration using an eddy covariance-based technique: improved assessment of soil moisture and land-atmosphere exchange dynamics. Vadose Zone J. https://doi.org/10.2136/vzj2012.0025

Scanlon TM, Sahu P (2008) On the correlation structure of water vapor and carbon dioxide in the atmospheric surface layer: a basis for flux partitioning. Water Resour Res 44:W10418. https://doi.org/10.1029/2008WR006932

Semmens KA, Anderson MC, Kustas WP, Gao F, Alfieri JG, McKee L, Prueger JH, Hain CR, Cammalleri C, Yang Y, Xia T, Sanchez L, Alsina MM, Vélez M (2016) Monitoring daily evapotranspiration over two California vineyards using Landsat 8 in a multi-sensor data fusion approach. Remote Sens Environ 185:155–170. https://doi.org/10.1016/j.rse.2015.10.025

Sun L, Gao F, Anderson MC, Kustas WP, Alsina M, Sanchez L, Sams B, McKee LG, Dulaney WP, White A, Alfieri JG, Prueger JH, Melton F, Post K (2017) Daily mapping of 30 m LAI, NDVI for grape yield prediction in California vineyard. Remote Sens 9:317. https://doi.org/10.3390/rs9040317

White AW, Alsina M, Nieto H, McKee L, Gao F, Kustas WP (this issue) Indirect measurement of leaf area index in California vineyards: utility for validation of remote sensing-based retrievals. Irrig Sci